Digest Journal of Nanomaterials and Biostructures Vol. 15, No. 1, January - March 2020, p. 133 - 141

DESIGN AND OPTIMIZATION OF PLATINIUM HEATERS FOR GAS SENSOR APPLICATIONS

A. A. ABDESLAM[a,b,*], K. FOUAD[a], A. KHALIFA[b]
[a]*MoDERNa laboratory, Department of Sciences and Technology, University of Frères Mentouri, Constantine 1, Constantine, Algeria*
[b]*IM2NP Laboratory, Aix Marseille Univ, Université de Toulon, Marseille, France*

A new bridge-type micro-hotplates (MHP) for semi-conducting metal oxide (SMO) gas sensor is investigated and its numerical study is simulated using Finite Element Method. the boundary conditions of the thermal properties have been calculated. The proposed MHP has been designed for low power consumption and uniform temperature distribution throughout the active area of 240 µm × 240 µm. To validate our simulation, we compared the results with the experimental data, reported by *Iwata et al*. The power consumption of the heater is approximately corresponded to 13.5 mW for heating to 300°C (heat transfer coefficients calculated), we noticed a reduction of power consumption by more than 8 mW compared to our first simulation (standard heat transfer coefficient parameters) which proves the impact of heat transfer coefficients on power consumption. Also, overheating problem in the heater center is analyzed, several modifications on the MHP center design have been established to keep the best temperature homogeneity, results show that temperature gap between extremities and the center of the active area is reduced by less than 15 °C.

(Received October 16, 2019; Accepted February 21, 2020)

Keywords: MEMS, COMSOL multiphysics, Gas sensor, MHP, Micro-hotplates, Heater geometry

1. Introduction

In the last few years there has been a growing interest in the number of applications for the MEMS with a heating element (MHP or heater), since they are key components in miniaturization of micro-sensors [1], such as wind sensors [2], humidity sensors [3] and gas sensors. The gas sensor with semiconducting metallic oxide (SMO) is becoming the universal MEMS sensor of the world due to its low congestion, high sensibility and fast answer. This sensor can be employed in several emergent applications such as sensors networks, label RFID, medical applications, quality surveillance food, portable devices, etc. [4, 5]. The amount of premature deaths around the world is about 7 million people per year (according to the World Health Organization) due to the effect of contaminants in the atmosphere. [6] Gas sensors are particularly important in preventing the spread of gases that are harmful to organic life and also in the detection of oxygen deficiencies in environments where they are required. [7] Nevertheless, an additional reduction of the energy consumption and the improved selectivity are always necessary to allow wide marketing of this innovative device. Nowadays, the lowest energy consumption in the sensors of gas marketed SMO is superior to 15mW when it is continuously exploited in 300°C [8-10].

The sensor of gas, which was nominated as a finalist in the annual price of creativity in electronics (ACE) 2017 (CCS811) has an energy consumption of 46 mW [11]. However, it is considered and intended for portable applications. The principle of functioning of the sensor of gas SMO rests on the heating of the layer of detection in temperature between 250°C and 550°C by using Joule effect. The required temperature of functioning depends on the used material of detection and on the type chap of targeted gas. To reach and maintain this temperature, the heater is the key device. Various materials such as the aluminum, the platinum [12, 13], the poly silicon

* Corresponding author: aimer.abdeslam@gmail.com

[14], the copper [15, 16], Gold [17], Nickel-Chromium (nor Cr) [18], Platinum Titanium [19], and Tungsten [20] can be used as a heater. The heater layer is supported by a dielectric membrane (SiO_2). This membrane acts as an electrical insulation that can operate under high temperatures. Metal oxides have been the most widely used materials for gas detection because of their ability to react with oxygen [21]. Among the most commonly used in the commercial market are tin dioxide (SnO_2), zinc oxide (ZnO), and tungsten trioxide (WO_3), as they meet all the requirements for good detection performance. In [21-24], gas is compared to others, such as In_2O_3, ITO, CdO, $ZnSnO_4$, Nb_2O_5 etc [25-27]. For this purpose, the design has been modeled using different structures in order to improve the power consumption, and temperature uniformity in the active area. These features are a crucial requirement for portable applications such as wearable athletic clothing, smart watches, and smart rings. The sensors are rigorously analyzed based on finite element simulations using COMSOL Multiphysics. The obtained results with the proposed design are discussed in the following sections.

2. Sensor structure and heater design

Fig. 1 presents different layers constituting the gas sensor. Platinum was used as heating element with a thickness of 0.1 µm. The heating film was supported by a 1×1 mm suspended membrane SiO2. In fact, the membrane is used as an electrical insulator at high temperature. This membrane has been designed to be thin (0.2 µm) in order to reduce conduction losses, and stable (low residual stress in the range of working temperature), and strong enough (strengthen by 8 beams) to carry the heater without risk of breaking.

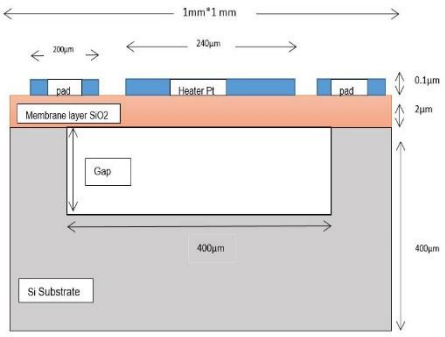

Fig. 1. Structure and layers constituting the gas sensor.

The choice of heater material is determined by an operating temperature range adapted to the needs, and good homogeneity on the active surface. Platinum (Pt) has various advantages such as lower density, good specific heat capacity, high electrical conductivity, etc. It is also a dense, malleable, ductile, precious. Thus, it is the least reactive metal. It also has very good specific heat and heating properties. By reducing the dimensions of the geometry, a higher temperature can be reached.

Table 1. Parameters used for simulations [1,21,24,25,28,32].

Material	*Density ρv ($kg.m^{-1}$)*	*Heat capacity at constant pressure Cp ($J.Kg^{-1}.K^{-1}$)*	*Thermal conductivity k ($W.m^{-1}.K^{-1}$)*	*Electric resistivity ρ (Ω.m)*
Si	*2330*	*713*	*156,0*	*$3,0.10^{8}$*
SiO2	*2270*	*1000*	*1,4*	*$1,0.10^{13}$*
Poly-Si	*3280*	*750*	*180,0*	*$1,5.10^{-05}$*
Pt	*21440*	*133*	*72,0*	*$3,4.10^{-07}$*

Table 1 summarizes the properties of materials used to build our gas sensor, and introduced in the parameters of COMSOL Multiphysics.

3. Electro-thermal analysis

To illustrate our model, a simulation was performed with COMSOL Multiphysics, it's a powerful interactive environment for modeling and solving all kinds of scientific and engineering problems based on Partial Differential Equations (PDEs), and its use does not require a deep knowledge of mathematics or numerical analysis, but the models are built on the basis of adequate physical characteristics equations [29].

We started by investigating the electro-thermal model to simulate the heating by the Joule eff ect. This model includes two modes: conduction mode with the continuity equation given in (1) and heat transfer mode described by (2) [30]. The Joule Heating Model node in COMSOL uses the following version of the heat equation as the mathematical model for heat transfer in solids:

$$-\nabla\,(-\nabla V)\;=\;0 \tag{1}$$

$$Q = \rho C_p \frac{dT}{dt} - \Delta(k.\Delta T) \tag{2}$$

These two equations are linked by the following equation for Joule heating [17]:

$$Q\;=\;\nabla V^2 \tag{3}$$

With the following material properties:
Q: Heat source (W/ m^3)
C_p: Heat capacity (J/kg. K)
T: Temperature (K)
ρ : Density (kg/m^3)
K: Thermal conductivity (W/m. K)

In Joule heating, the temperature increases due to the resistive heating from the electric current. The electric potential V is the variable solution in the conductive media DC application mode. The generated resistive heat Q is expressed as:

$$Q = \rho|J^2| \tag{4}$$

where σ *is* Electric conductivity and *J* is the current density, which is also the reciprocal of the temperature dependent electric conductivity.

$$\sigma = \sigma(T) \tag{5}$$

Combining these facts gives the fully coupled relation.

$$Q = \frac{1}{\sigma}|J^2| = \frac{1}{\sigma}|\sigma E|^2 = \sigma|\Delta V|^2 \tag{6}$$

Over a range of temperatures, the electric conductivity σ is a function of temperature T.

$$\sigma = \frac{\sigma_0}{1 + \alpha(T - T_0)} \tag{7}$$

where σ_0: the conductivity at the reference temperature T_0, α is the temperature coefficient of resistivity, which describes how the resistivity varies with temperature.

Besides, the power consumption is described as:

$$P = \frac{V^2}{R} \tag{8}$$

with the following material properties:
where V is voltage and R stands for the resistance of the heating electrode. Here power consumption is directly proportional to the applied voltage and inversely proportional to the resistance of the material. The equations have been solved numerically under mixed boundary conditions (Dirichlet and Neumann), using the finite element method in COMSOL [31]. Fixed temperature and potentials are assumed at ends of the heater.

A lot of materials properties are required to solve the mathematical equations mentioned above. In Table1 material properties of platinum are shown.

Several thermal transfer phenomena in materials and at borders have been taken into account during simulations. There is thermal conduction in the solid material, natural convection at the boundaries between solids and air and radiation. According to previous studies [28, 23, 30], heat transfer coefficients are usually set as 125 $Wm^{-2}K^{-1}$for the surface and side walls of the chip and 60 $Wm^{-2}K^{-1}$for the back side of the membrane. Therefore, in this study we calculated the heat transfer coefficients particularly for our model in order to get the closest possible to reality and to improve the temperature homogeneity. The conduction of the different tested materials was parameterized in the 3D parts of the model. Knowing that platinum conduction is high so it must therefore be set as a "highly conductive" layer. There is a natural convection to the walls when the support is heated in the air. This convection phenomenon comes into play in thermal equilibrium and influences the value of the temperature. It is therefore important to take it into consideration; regarding the upper surface of the lid, we have a horizontal plane in the air with the convective effect going upwards. Heat transfer coefficient is calculated using the following equation:

$$h = 1{,}32 \times \left(\frac{\Delta\theta}{1}\right)^{0,25} \tag{9}$$

Implies that,

$$h(T) = 1{,}32 \times \left(\frac{T - T_0}{1{,}36}\right)^{0,25}$$

with T_0=293K

This equation depends on the number of Nusselt (Nu) (eq.9), which from one side depends on the flow regime along the support walls that are considered laminar; and from other side depends on the geometry that is defined by the length of the device as well as the orientation towards the top of the heating face:

$$Nu = C.(Ra)^n \tag{10}$$

With n=0,25

$$Ra = Gr.Pr \tag{11}$$

With $Gr = \frac{l^3\rho^2 g\beta\,\Delta\theta}{\mu^2}$
And Pr = 0,707
l = length of the plate
ρ=density
g=gravity acceleration
β=coefficient of expansion =1/T_K in the case of air
$\Delta\theta$=temperature difference
Ra=Rayleigh number

Pr=Prandtl number

Gr= Grashof number

The calculation of the Rayleigh number made possible to determine the constants used to calculate the Nusselt number, and to determine the shape of the equation of the convective transfer coefficient:

$10^2 < Ra < 10^4$ according to the temperature and so

$$h = 1{,}32 \times \left(\frac{\Delta\theta}{1}\right)^{0{,}25} \qquad \text{(eq.9)} \qquad [32]$$

The value of the thermal coefficient h for the plate is between 10 and 20 depending on the temperature. For the condition at the interface between the bottom of the substrate and the air we have chosen in a first step to define a total thermal insulation. This seemed necessary to get rid of the base on which the substrate will be placed and therefore to be placed in an ideal case. This also allows for a minimum of heat loss and a more reliable comparative result between materials.

The effects of radiation in heat transfer must also be taken into account. The silicon emissivity was considered to be 0.37 according to the article by *Böhnke et al* [33]. For the sake of precision, neighbouring emissivity values of 0.32 and 0.42 were also tested. It was then noticed that this possible difference only slightly influenced the result of the simulation.

4. Electro-thermal simulation of the MHP

The choice of our heater design for the suite was the spiral shape since it provides a good compromise between good temperature homogeneity and low power consumption, and also to avoid thermal stress in the angles of the heater tracks. A new membrane shape was used as part of the 8 micro-bridges design to provide better insulation against heat loss from the heater to the substrate. This results in minimizing heat dissipation and reducing power consumption up to a few mW.

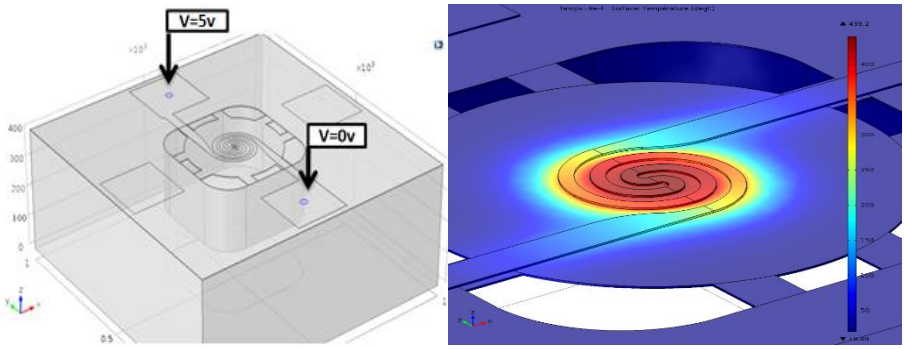

(a) *(b)*

Fig. 2. a) Gas sensor without measuring electrodes b) Heater temperature under 5V op applied tension.

The modifications made to the sensor design are:

• The addition of membrane etching with bridges to connect the heater's tracks to the pads to minimize the heat generated by the substrate.

• Used the circular spiral shape as a design with a track width of 10µm, similarities between the tracks.

• A modification was made to the width between the tracks of the heater ranging from 12µm (centre of the active area) to 8µm (the end of the active area) as shown in Fig. 3.

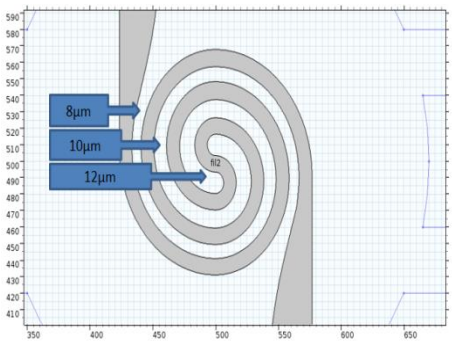

Fig. 3. Changing the width of the heater tracks.

• The spacing between the tracks of the heater was limited to 8µm in order to introduce the measuring electrodes in the next step, this will allow us to avoid the addition of another layer above the heater for the sensor electrodes that will be on the same level as the heater, which reduces the manufacturing cost of our sensor.

• Round off the connections of the heater in a gradual way, for the fluidity of the current that reaches the active area from the pads.

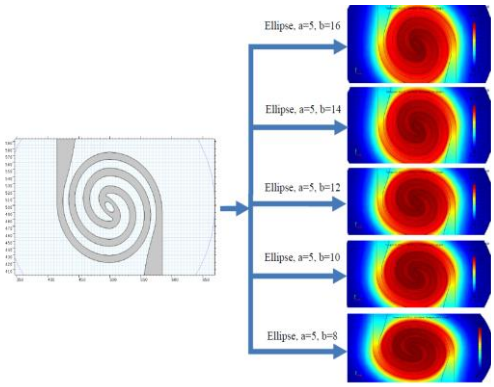

Fig. 4. Adding an elliptical hole to the center track of the heater (a and b in µm).

Despite this improvement, the temperature difference between the center and extremities in the active area remains important. to solve this problem, we suggest replacing two half-circles located at the MHP center with an elliptical shape, given in Figure 4. This is done by supplying 2 volts.

To reduce the concentrated temperature in the middle of the MHP, we must keep a uniform current density in the heater, for this we must keep the same width of tracks which does not apply to the case of the ellipse. Therefore, a hole in the ellipse is suggested so that the current density remains stable over the entire track of the heater as shown in Fig. 4.

5. Results and discussions

Fig. 5 presents a parametric comparison between different dimensions of the elliptical hole in the center track of the heater, where ‘a’ represents the horizontal diagonal of the elliptical hole, and ‘b’ is the vertical diagonal. ‘a’ is fixed at 5µm, while ‘b’ takes different values from 16µm to 8µm.

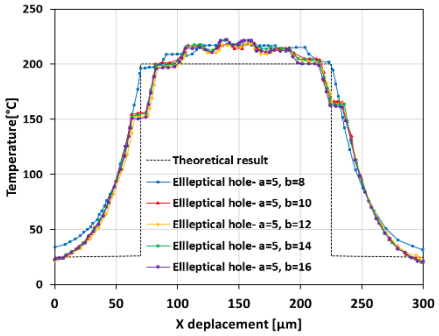

Fig. 5. The temperature [°C] versus layer position in device for different axes (a, b) of elliptical hole in the center track of the heater.

The results show that the elliptical hole with a=5, b=8 is the one that matches the most the theoretical graph (ideal homogeneity), which illustrates the perfect uniformity of temperature in the active area (70µm to 225µm). In the case of the blue graph (a=5, b=8), it has been noticed that temperature gap between extremities and the center of the active area is reduced by less than 15 ° C, which is very promising to improve the signal to noise ratio, this result is due to the equality between the current density in the platinum track (10µm) and the sum of the current densities in the two sides of the elliptical area.

As can be seen from Fig. 6, the temperature was plotted against the corresponding power consumption. The red graph presents our first simulation using standard parameters of the heat transfer coefficient [28, 23, 29]. The blue one shows our simulation when heat transfer coefficients are calculated, specifically for our model as shown in section 4, taking into account the boundary conditions and the geometrical parameters. the graph in black is the experimental result of [28].

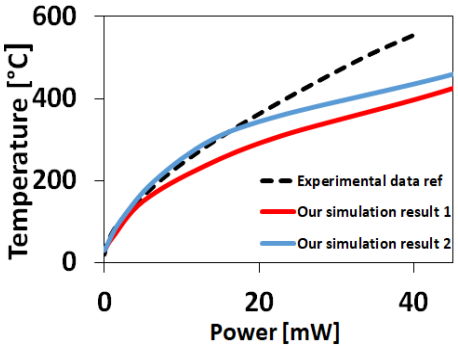

Fig. 6. A comparison between the power consumption of our simulation results and the experimental result of [28].

The power consumption during the heating MHP to 300 °C was approximately 13.4 mW, these modifications allowed us to gain 8 mW less in power consumption compared to our first simulation, and 0.6 mW compared to [28] and also to have a better uniformity in the active area. This difference power values can be explained by the calculations of heat transfer coefficients, MHP and membrane design, and Geometric modifications contributed to the heater.

Our sensor is designed to work in environments when temperature is lower than 300°C this is why for temperatures above 300 ° C, it is noticed that power consumption on the MHP of [28] is lower than our two models, this can be explained by the improvements that he made in his work on the membrane with adding an SU-8 layer on his MHP, this allows him to have a stable operation under a constant voltage for 100 min.

6. Conclusions

The aim of this paper was to simulate several solutions to improve the homogeneity of the temperature provided by the heating element, while miniaturizing the geometry of the sensor, and to develop a new design that minimizes the power consumption compared to the sensors of the literature. This work has been done under the simulation software COMSOL Multi-physics.

Several simulations have been addressed to keep the best homogeneity along the active zone of our gas sensor design studies, the different phenomena that govern the sensor, design of the membrane, also on the track of the heater and the measuring electrodes. Moreover, a new design of semiconductor metal oxide gas sensors that implement several innovative aspects to further reduce overall energy consumption, while improving thermal uniformity in the active area and the movement of energy was proposed.

References

[1] N. Dufour, Technological improvements of a metal oxide gas multi-sensor based on a micro-hotplate structure and inkjet deposition for an automotive air quality sensor application, 25th Micromechanics and Microsystems Europe workshop, Istanbul, Turkey. 4p (2014). [online]. https://hal.archives-ouvertes.fr/hal-01058911

[2] F. Mailly, A. Giani, R. Bonnot, P. Temple-Boyer, F. Pascal-Delannoy, A. Foucaran, A. Boyer, Sens. Actuat. A **94**, 32 (2001).

[3] C. L. Dai, Sens. Actuat. B **122**, 375 (2007).

[4] Kourosh Kalantar-Zadeh et al., Gastroenterology **150**(1), 37 (2016).

[5] Estefania Abad, et al., Sensors and Actuators B: Chemical **127**(1), 2 (2007).

[6] https://www.who.int/airpollution/en

[7] A. Adeyemo, J. Mathew, J. Comput. Electronics **17**, 1285 (2018).

[8] TGS 8100 {for the detection of Air Contaminants, FIGARO USA, Inc., Arlington Heights, USA. [online]. http://www.figarosensor.com/products/entry/tgs8100.html

[9] CCS801 {Ultra-Low Power Analog VOC Sensor for Indoor Air Quality Monitoring, AMS AG, Unterpremstatten, Austria. [online]. http://ams.com/eng/Products/Environmental-Sensors/Gas-Sensors

[10] SGP30 {Sensirion Gas Platform, Sensirion, Staefa, Switzerland. [online]. https://www.sensirion.com/en/environmental-sensors/gas-sensors/

[11] 2017 Annual Creativity in Electronics Awards Announces Finalists from Leading Companies, Design Teams, and Executives in the Electronics Industry. [online]. http://ubm-tech.mediaroom.com/index.php?s=17177&item=138045

[12] G. Velmathi, N. Ramshanker, S. Mohan, Excerpt from the Proceedings of the COMSOL Conference, India, Oct. 29–30 (2010).

[13] T. M. Hsieh, C. H. Luo, F. C. Huang, J. H. Wang, L. J. Chien, G. B. Lee, Sensors and Actuators B: Chemical **130**(2), 848 (2008).

[14] L. Sujatha, V. S. Selvakumar, S. Aravind, R. Padamapriya, B. Preethi, Excerpt from the Proceedings of the COMSOL Conference, Bangalore (2012).

[15] A. Botau, D. Bonfert, C. Negrea, P. Svasta, C. Ionescu, Electro-Thermal Analysis of Flexible Micro-Heater, 38th International Spring Seminar on Electronics Technology. (2015). [online]. https ://doi.org/10.1109/isse.2015.72480 22

[16] H. J. Pandya, Chandra Sudhir, A. L. Vyas, Sensors and Actuators B: Chemical **161**(1), 923 (2012).

[17] Y. S. Kim, Sensors and Actuators B: Chemical **114**(1), 410 (2006).

[18] S. Das, J. Akhtar, J. «Comparative Study on Temperature Coefficient of Resistance (TCR) of the E-beam and Sputter Deposited Nichrome Thin Film for Precise Temperature Control of Microheater for MEMS Gas Sensor, » In: Jain, V., Verma, A. (eds) Physics of Semiconductor Devices. Environmental Science and Engineering. Springer, Cham (2014). [online]. https://doi.org/10.1007/978-3-319-03002-9_124016

[19] T. Guan, R. Puers, Procedia Engineering **5**, 1356 (2010).

[20] P. Menini, Du capteur de gaz a oxydes métalliques vers les nez électroniques sans fil, Ph.D. dissertation, Paul Sabatier University, France (2012).
[21] Mahanth Prasad, Vineet Sahula, Vinod Kumar Khanna, IEEE transactions on semiconductor manufacturing **26**(2), 233 (2013).
[22] G. E. Patil et al., Spray pyrolysis deposition of nanostructured tin oxide thin films, ISRN Nanotechnology (2012).
[23] A. Bouaoud et al., Materials Chemistry and Physics **137**(3), 843 (2013).
[24] D. Punetha, H. Dixit, J. Comput. Electronics, https://doi.org/10.1007/s10825-018-1269-7 (2018).
[25] E. Li et al., Crystal Growth and Design **9**(5), 2146 (2009).
[26] Rozina Abdul Rani et al., Sensors and Actuators B: Chemical **176**, 149 (2013).
[27] H. Zhongqiu, Ph.D. Thesis, Department of Molecular and Material Sciences Interdisciplinary Graduate School of Engineering Sciences, Kyushu University (2014).
[28] T. Iwata, W. P. C. Soo, K. Matsuda, K. Takahashi, M. Ishida, K. Sawada, J. Micromech. Microeng. **27**, (2017).
[29] K. Saleh, Geometry effect of suspended membrane on the sensitivity of pressure sensor field effect transistor (PSFET), Proceedings of the International Conference on Recent Advances in Electrical Systems, Tunisia (2017).
[30] V. Bansal, A. Gurjar, D. Kumar, B. Prasad, Excerpt from the Proceedings of the COMSOL Conference, Bangalore (2011).
[31] B. Souhir, Design and Simulation of Microelectromechanical Systems (MEMS) for Ozone Gas Sensors, The Korean Institute of Electrical and Electronic Material Engineers, ISSN 2092 (2018).
[online]. https://doi.org/10.1007/s42341-018-0001-4
[32] B.T. Marquis, J. F. Vetelino, Sensors and Actuators B **77**, 100 (2001).
[33] T. Böhnke, H. Kratz, A. Hultaker et al., Optical Materials **30**, 1410 (2008).